



ISSN: 2447-3359

REVISTA DE GEOCIÊNCIAS DO NORDESTE

Northeast Geosciences Journal

v. 6, nº 2 (2020)

<https://doi.org/10.21680/2447-3359.2020v6n2ID21687>



DISTURBANCES IN THE GEOMAGNETIC FIELD DUE TO THE EARTHQUAKE AND TSUNAMI OF MAULE, CHILE (2010)

Virginia Klausner¹; Marina Vedelago Cezarini²;
Thiago de Almeida Santos³

¹Doctor in Geophysics, Department of Physics and Astronomy, University of Vale do Paraíba (UNIVAP), São José dos Campos/SP, Brasil.

ORCID: <https://orcid.org/0000-0003-0250-5574>

Email: viklausner@gmail.com

²Undergraduate student in Electrical Engineering, University of Vale do Paraíba (UNIVAP), São José dos Campos/SP, Brasil., University of Vale do Paraíba (UNIVAP), São José dos Campos/SP, Brasil.

ORCID: <https://orcid.org/0000-0003-1389-3293>

Email: marina.cezarini@gmail.com

³Undergraduate student in Electrical Engineering, University of Vale do Paraíba (UNIVAP), São José dos Campos/SP, Brasil.

ORCID: <https://orcid.org/0000-0003-3709-2685>

Email: thiagoalmeidamusico@hotmail.com

Abstract

This study analyzes the disturbances in the geomagnetic field related to the earthquake, and the consequent tsunami, which occurred on February 27, 2010, in Maule, Chile. The purpose of this article is to contribute to a better understanding of the physical processes involved in the Tsunami-Atmosphere-Ionosphere (TAI) and Lithosphere-Atmosphere-Ionosphere (LAI) couplings. To this end, records of fluxgate magnetometers measured on the surface provided by the LISN project (Low Latitude Ionospheric Sensor Network) were used. The methodology of signal filtering by removing the Sq baseline (related to the Solar Quiet variabilities) considering the five geomagnetically quieter days was applied. In both the H and Z components, the results show geomagnetic disturbances in the filtered data that occurred almost instantly or with a delay of up to 100 minutes after the tsunami's arrival. These disturbances are attributed to be of oceanic and ionospheric origin. Studies like this are important to a future prediction condition and early warning of disasters of this nature.

Keywords: Tsunami; Earthquake; Wave propagation.

PERTURBAÇÕES NO CAMPO GEOMAGNÉTICO CAUSADAS PELO TERREMOTO E PELO TSUNAMI DE MAULE (2010)

Resumo

Este estudo foca na análise das perturbações do campo geomagnético que estão relacionadas com o terremoto, e consequente tsunami, que ocorreram em 27 de fevereiro de 2010 em Maule, no Chile. O objetivo deste artigo é contribuir para uma melhor compreensão dos processos físicos envolvidos nos acoplamentos Tsunami-Atmosfera-Ionosfera (TAI) e Litosfera-Atmosfera-Ionosfera (LAI). Para isto, foram utilizados registros de magnetômetros *fluxgate* medidos em superfície fornecidos pelo projeto LISN (do inglês *Low Latitude Ionospheric Sensor Network*). A metodologia de filtragem do sinal por remoção da tendência relacionada à influência solar (linha de base Sq, do inglês *Solar quiet*) considerando os cinco dias geomagneticamente mais calmos foi aplicada. Os resultados mostraram distúrbios geomagnéticos, em ambas componentes H e Z, nos dados filtrados que ocorreram quase instantaneamente ou com atraso de até 100 minutos após a chegada do tsunami. Estes distúrbios são atribuídos aos mecanismos oceânico e ionosférico. Estudos como esse são importantes para uma futura condição de previsão e alerta de desastres dessa natureza.

Palavras-chave: Tsunami; Terremoto; Propagação de ondas.

PERTURBACIONES EN EL CAMPO GEOMAGNÉTICO CAUSADAS POR EL TERREMOTO Y POR EL TSUNAMI DE MAULE, CHILE (2010)

Resumen

El presente estudio se centra en el análisis de las perturbaciones del campo geomagnético que están relacionadas con el terremoto y el consiguiente tsunami, que ocurrió el 27 de febrero de 2010 en Maule, Chile. El propósito de este análisis es contribuir a una mejor comprensión de los procesos físicos involucrados en los acoplamientos Tsunami-Atmósfera-Ionosfera (TAI) y Litosfera-Atmósfera - Ionosfera (LAI). Para esto, se utilizaron registros de magnetómetros *fluxgate* medidos en la superficie, proporcionados por el proyecto LISN (del inglés *Low Latitude Ionospheric Sensor Network*). Para este análisis, se utilizó la metodología de filtrado de la señal mediante la eliminación de la tendencia relacionada con la influencia solar (línea base Sq, del inglés *Solar quiet*) considerando los cinco días

geomagnéticamente más tranquilos. Los resultados muestran perturbaciones geomagnéticas, tanto en componentes H como Z, en los datos filtrados que ocurrieron casi instantáneamente o con un retraso de hasta 100 minutos después de la llegada del tsunami. Estas perturbaciones se atribuyen a los mecanismos oceánico e ionosférico. Estudios como este son importantes para una condición futura de pronóstico y advertencia de desastres de esta naturaleza.

Palabras-clave: Tsunami; Terremoto; Propagación de ondas.

1. INTRODUCTION

Tsunamis are long-wavelength waves that can be generated by geophysical events such as earthquakes, volcanic eruptions, and landslides. However, they are usually generated by earthquakes of tectonic origin, produced by the convergent movement of lithospheric plates. This movement is known as subduction, in which a denser lithospheric plate "dives" under another less dense. Two other movements also produce earthquakes, these being the divergent and transforming movements. The divergent movement consists of the spacing between lithospheric plates, in which earthquakes may occur at their borders. The transformer, on the other hand, is due to the shear movement at the boundary between plates (TEXEIRA et al., 2009).

During the occurrence of an earthquake in coastal and oceanic regions, deformation of the ocean floor occurs, and this deformation is directly related to the dimensions of the vertical displacement of the seabed. As a result of the vertical displacement of the water column, the displacement of the ocean surface occurs, generating concentric waves that propagate in all directions until the system returns to its equilibrium again. Tsunamis begin as wavelength waves in the order of hundreds of kilometers. In deep waters, these waves spread rapidly, crossing the oceans at speeds between 600 and 800 kilometers per hour, but with amplitudes of only a few tens of centimeters above the sea surface, passing almost unnoticed by boats and ships. However, when they reach the coast, the change in depth produces a transformation: their wavelength diminishes, their speed drops, and, most impressively, their amplitude increases, reaching tens of meters.

On February 27, 2010, at 06:34 UT, an earthquake with Mw 8.8 and epicenter located at -35.85° in Latitude and -72.72° in Longitude, and focal depth of 35 km generated a tsunami that spread across the Pacific Ocean region with 26-meter waves heading towards the city of Maule, central coast of Chile. In this work, the geomagnetic data related to this event will be analyzed, to detect disturbances in the geomagnetic field caused by the tsunami and the earthquake. Seismic and oceanic mechanisms will also be discussed. To this end, a methodology for filtering magnetic variations with seismogenic and oceanic forcing was developed in an extremely quiet geomagnetic period.

A geomagnetically quiet period is associated with variations in electric currents in the ionosphere in a steady-state, and in this way, one can analyze the behavior of these currents before a local external forcing. In this case, the external electric field may have been induced by ocean currents or by gravity waves (GWs),

which will be discussed further. These ionospheric currents are called Sq currents (Sq stands for Solar Quiet).

2. SEISMIC MECHANISM

During an earthquake, two types of body waves are generated: P or compression waves, which are longitudinal pressure waves (Figure 1a). These waves have small amplitudes, propagate in any medium, and, in the earth's crust, they have speeds of ~ 6 km/s; and S or shear waves, which are transversal (Figure 1b), present amplitudes several times greater than the P waves, travel only in solid media, and have speeds of ~ 3.6 km/s (60% of the speed of the P waves).

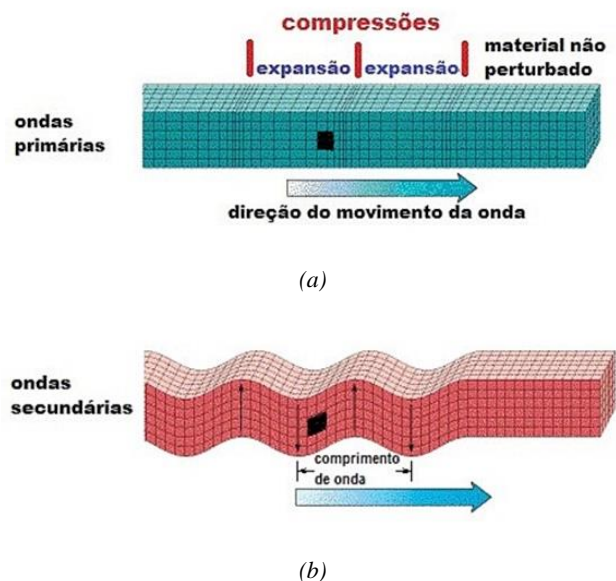


Figure 1 - Representation of body waves, in which (a) is the propagation of P or compression waves, and (b), S or shear waves, respectively. Source: Medeiros, Alexandre (2001).

The interaction between P and S waves generates two types of surface waves: Rayleigh waves, which propagate as if they were "ripples" (Figure 2a) and have speeds of ~ 3.4 km/s (90% of the speed of the S waves); and Love waves, which are horizontally polarized shear waves (Figure 2b), with speeds slightly higher than the Rayleigh waves. The S and Rayleigh waves, as previously described, oscillate in a direction perpendicular to their direction of propagation, and consequently, they are capable of strongly shaking the atmosphere above due to the vertical displacement of the Earth's surface (LOGNONNÉ et al., 2006). Atmospheric waves are generated, propagating to ionospheric altitudes, producing ionospheric disturbances (Travelling Ionospheric Disturbances - TIDs) that induce electric and magnetic fields. Therefore, the lithosphere-atmosphere-ionosphere (LAI) coupling mechanism occurs through collisions between particles from the neutral atmosphere and electrons from the ionized portion of the Earth's atmosphere, the ionosphere.

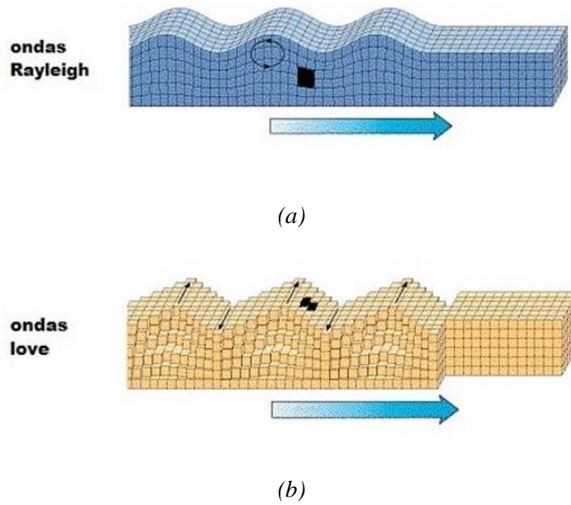


Figure 2 - Representation of surface waves, in which (a) is the propagation of Rayleigh waves, and (b), Love waves, respectively. Source: Medeiros, Alexandre (2001).

The propagation of acoustic gravity waves (AGWs) at ionospheric altitudes generates an electric field due to the polarization, arising from the dynamo current in the ionospheric E region, in the East-West direction over the epicenter. In turn, this electric field is mapped by the magnetic field lines up to ionospheric altitudes. Thus, electric fields end up being generated due to ionospheric currents, both in the East-West direction and in the North-South direction, due to the ionospheric electrical conductivities Pedersen and Hall, respectively (IYEMORI et al., 2005).

After an earthquake, the S and Rayleigh waves are the first to disturb the atmosphere. AGWs are generated by a tsunami or earthquake and have a speed of up to 800 m/s. Following these waves, the GWs arises, and these generally have the same speed as the tsunami waves, about 200 m/s. The GWs can also propagate to ionospheric altitudes. In addition to these mechanisms described above, the propagation of AGWs at ionospheric altitudes can generate secondary GWs. Figure 3 illustrates the generation and propagation of GWs, AGWs, and secondary GWs due to earthquake and tsunami.

The Tsunami-Atmosphere-Ionosphere (TAI) coupling mechanism has three stages: (a) generation of the tsunami wave by seismic rupture; (b) generation of GWs/AGWs by tsunami waves; and (c) subsequent excitation of ionospheric disturbances by GWs/AGWs (similar to the LAI mechanism). The GWs and AGWs have periods of < 270 s, and > 270 s to 3 hrs, respectively (KHERANI et al., 2012). The following equations were described by Navier-Stokes regarding the movement of the atmosphere.

$$\frac{\partial \vec{w}'}{\partial t} + (\vec{w}' \cdot \nabla) \vec{w}' = -\frac{1}{\rho_m} \nabla p + \vec{g} + \frac{\mu}{\rho_m} \nabla^2 \vec{w}' + \vec{F}_{cor}, \quad (1)$$

$$\vec{w}' = \vec{w} + \vec{w}_0, \quad (2)$$

$$\frac{\partial \rho_m}{\partial t} + \nabla \cdot (\rho_m \vec{w}) = 0, \quad \text{and} \quad (3)$$

$$\frac{\partial p}{\partial t} + (\vec{w}' \cdot \nabla) p + \gamma p (\nabla \cdot \vec{w}') = 0, \quad (4)$$

where \vec{w} is the disturbed wind, \vec{w}_0 is the "background" wind, ρ_m , γ , \vec{w} , p are the density, the adiabatic constant, the wind and the atmospheric pressure, respectively. Furthermore, \vec{g} is the gravitational acceleration, μ is the dynamic viscosity, e \vec{F}_{cor} is the Coriolis force.

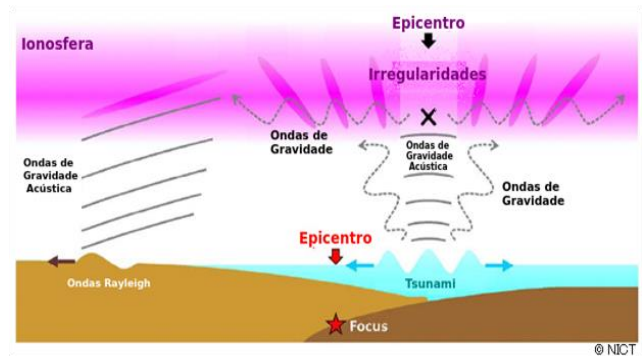


Figure 3 - Scheme of the ionospheric wave generation mechanisms. Source: Modified from Tsugawa (2011).

AGWs are generated by forcing forces that can alter atmospheric pressure, such as seismic activities, that is, volcano/earthquake/tsunami; and meteorological activities, such as hurricanes, tropospheric convections, and rainfall. In other words, the forces \vec{g} e $-\nabla p$ and the inertial force $d\vec{w}'/dt$ are related to the generation of GWs/AGWs. To analyze mathematically the distribution ratio of GWs/AGWs, one must consider that there is no energy dissipation, the two-dimensional plane wave solution equated as $e^{(\omega t - k_x X + k_z Z)}$, and small oscillations in terms of density and pressure. With the conditions described above, we have

$$\omega \geq \omega_a, \quad \omega = \gamma \frac{\vec{g}}{\vec{v}_{som}}, \quad (5)$$

$$\omega \leq \omega_b, \quad \omega = (\gamma - 1)^{1/2} \frac{\vec{g}}{\vec{v}_{som}}, \quad (6)$$

where ω_a e ω_b represent the frequency of acoustic resonance and Brunt-Väisälä, respectively. Besides, ω is the angular frequency, e \vec{v}_{som} is the speed of sound. Finally, equation 7 describes the dispersion of GWs/AGWs for the conditions described in equations 5 and 6.

$$\omega^4 - \omega^2 \left[\vec{v}_{som}^2 (k_x^2 + k_z^2) + (\gamma \vec{g} / 2 \vec{v}_{som})^2 \right] + (\gamma - 1) \vec{g}^2 k_x^2 = 0, \quad (7)$$

where γ is the ratio between the specific heats for atmospheric gas, and k_x e k_z are the wave numbers ($k = 2\pi/\lambda$) in the horizontal and vertical directions, respectively.

In summary, the atmosphere-ionosphere coupling occurs due to the neutral wind in the atmosphere that can generate movement of the ionospheric plasma by disturbances. And in the case of the LAI or TAI coupling, it occurs due to the wind disturbed by waves

Moreover, the movement (\vec{u}) of the ions generate ionospheric electric current (\vec{J}_w) which leads to an accumulation of charges, since the current gradient (\vec{J}_w) is different from zero, see equations 8, 9, 10, 11 and 12 below. Because this plasma does not allow this to happen, an electric field (\vec{E}) is generated, and it directs a current in the opposite direction ($\sigma\vec{E}$), since $\nabla \cdot (\vec{J}_w + \sigma\vec{E}) = 0$. Finally, the resulting movement (\vec{V}) is determined by this electromotive field and the wind, in addition to other forces, such as the gravitational force and the pressure force. The hydro-magnetic equations below represent the processes described above

$$\frac{\partial \vec{u}_s}{\partial t} = \frac{q_s}{m_s} (\vec{E} + \vec{u}_s \times \vec{B}_0) - \nu_s \vec{u}_s + \nu_s \vec{W}, \quad (8)$$

$$\frac{\partial n_s}{\partial t} + \nabla \cdot (n_s \vec{u}_s) = P_s - L_s, \quad (9)$$

$$\vec{J} = \vec{J}_w + \sigma \vec{E}; \quad \vec{J}_w = qn(\vec{u}_i - \vec{u}_e), \quad (10)$$

$$\nabla^2 \vec{E} - \nabla(\nabla \cdot \vec{E}) - \frac{1}{c^2} \frac{\partial^2 \vec{E}}{\partial t^2} - \mu_0 \frac{\partial \vec{J}}{\partial t} = 0, \quad \text{and} \quad (11)$$

$$\nabla^2 \vec{B} - \frac{1}{c^2} \frac{\partial^2 \vec{B}}{\partial t^2} = \mu_0 \nabla \times \vec{J}, \quad (12)$$

where $s = \text{ions } (i) \text{ or electrons } (e)$, q is the total electrical charge, m is the mass, n is the numerical density, ν is the frequency of collisions, c is the speed of light in a vacuum, μ_0 is the vacuum permeability, \vec{B}_0 is the Earth's magnetic field, P denotes the rate of ion and electron production and L is the loss rate, σ is the ionospheric electrical conductivity, \vec{J} , \vec{E} e \vec{B} are the electrical current density, the electric and magnetic fields in the ionosphere, respectively (KHERANI et al., 2012).

3. OCEANIC MECHANISM

Faraday (1922) predicted that ocean waters' movement could induce electric fields, a phenomenon called "motion induction." The salts dissolved in seawater are composed of ions that can have their movements altered by the Lorentz force that acts in a direction perpendicular to the fluid velocity vectors, \vec{V} , and magnetic field, \vec{B} (TYLER et al., 2003; MANOJ et al., 2006). As a consequence of this movement of seawater, a conduction current \vec{J} is produced, being expressed by

$$\vec{J} = \sigma_0 (\vec{E} + \vec{V} \times \vec{B}), \quad (13)$$

where σ_0 is the electrical conductivity of seawater, \vec{E} is the electric field using the reference system in the ocean, $e \vec{V} \times \vec{B}$ is the induced electric field. Disregarding any displacement current $\varepsilon = d\vec{E}/dt$, where ε is the electrical permittivity of the medium, Ampère's law can be used to determine an induced magnetic field \vec{B} given by

$$\vec{V} \times \vec{B} = \mu_0 \vec{J}, \quad (14)$$

where μ_0 is the magnetic permeability of the vacuum.

Faraday's law describes the induced electric \vec{E} and magnetic \vec{B} fields as

$$\nabla \times \vec{E} = -\frac{\partial \vec{B}}{\partial t}. \quad (15)$$

Maxwell's law for magnetic flux states that

$$\nabla \cdot \vec{B} = 0. \quad (16)$$

In this context, to determine the magnetic field vector induced by the oceans, we use the approach made by Tyler (2005), described by the following equations 17 to 22. The equation of the induced magnetic field given by

$$\frac{\partial \vec{B}}{\partial t} = \nabla \times (\vec{V} \times \vec{B} - K \nabla \times \vec{B}), \quad (17)$$

where $K = (\mu_0 \sigma_0)^{-1}$ is the magnetic diffusion coefficient.

Considering the gravity vector \vec{g} as a constant scalar field in the radial direction to the center of the Earth, and with spherical symmetry, given by $\vec{g} = -\nabla\theta$, and calculating the product scale between \vec{g} and equation 17, we have

$$\vec{g} \cdot \frac{\partial \vec{B}}{\partial t} = \nabla \cdot [(\vec{V} \times \vec{B}) \times \vec{g} - K(\nabla \times \vec{B}) \times \vec{g}]. \quad (18)$$

Considering that H stands for the component perpendicular to the radial component and the Z stands for the component parallel to the radial component, equation 18 can be rewritten as

$$\frac{\partial B_Z}{\partial t} + \nabla_H \cdot (B_Z \vec{V}_H) = \nabla_H \cdot (V_Z \vec{B}_H) + \nabla_H \cdot (K \nabla_H B_Z - K \frac{\partial \vec{B}_H}{\partial t}), \quad (19)$$

where $\vec{B}_H = \vec{B}_X + \vec{B}_Y$.

Assuming that $|V_H| \gg |V_Z|$ and decomposing $\vec{B} = \vec{F} + \vec{b}$, where \vec{F} is the total geomagnetic field (where $\nabla \times \vec{F} = \vec{0}$ and $\nabla^2 \times \vec{F} = 0$) and \vec{b} is the magnetic field induced by the oceans, equation 19 becomes

$$\frac{\partial b_Z}{\partial t} = -\nabla_H \cdot (F_Z \vec{V}_H) + \nabla_H \cdot (K \nabla_H b_Z - K \frac{\partial \vec{b}_H}{\partial t}), \quad (20)$$

where $\vec{b}_H = \vec{b}_X + \vec{b}_Y$.

If K is uniform throughout the ocean, and given by $K = K(Z)$, by applying equation 14, equation 20 can be simplified as

$$\frac{\partial b_z}{\partial t} = -\nabla_H \cdot (F_z \vec{V}_H) + K \nabla^2 b_z. \quad (21)$$

Ocean flow can occasionally be disturbed by tsunamis that cause a few centimeters per second increase in the speed \vec{V}_H of ocean wave propagation. Consequently, if this velocity \vec{V}_H increases, as shown in equation 13, the conduction current \vec{j} will also increase, which is closely related to an increase in the variation of the induced magnetic field \vec{b} , see equation 14.

As mentioned by Tyler (2005), the dynamics of oceanic flow during the propagation of tsunamis can be described as the propagation of surface gravity waves with long periods. To describe these waves, Tyler (2005) considered that:

1. The velocity \vec{V}_H does not depend on the variation in the depth of the ocean floor and varies more rapidly horizontally than in other parameters. The same occurs with \vec{b} . This is equivalent to assuming that the tsunami wavelength, although much greater than the depth of the ocean floor, is much smaller than the scale of variations of the F_z component. These considerations are valid for regions far from the coast, that is, the deep ocean.
2. Regions outside the ocean are electrically isolated, so $k \rightarrow \infty$ e $\nabla^2 b_z = 0$.
3. In the ocean, K can be represented by the average depth value, showing only very smooth variations in its horizontal component.

Taking these considerations, equation 21 can be applied within the limits of the ocean and $\nabla^2 b_z = 0$ for the region outside those limits. At the interface, due to the continuity conditions of b_z e $\nabla \cdot \vec{B} = 0$, the solutions must be the same. Since this interface is flat, the b_z component can be calculated using its Fourier transform (FT), $F_z \vec{V}_H \alpha e^{-i(\omega t - kx)}$, where ω is the angular frequency, k is the wave number e x is the position variation in the horizontal direction. This implies an estimated solution for the regions above the sea surface, where $Z \geq 0$, equal to

$$b_z = \frac{\sinh(\alpha h/2)}{\alpha K (\alpha \sinh(\alpha h/2) + k \cosh(\alpha h/2))} \nabla \cdot (F_z \vec{V}_H) e^{-kZ}, \quad (22)$$

where $\alpha = (k^2 - i\omega/k)^{\frac{1}{2}}$, $k = |k|$, $\vec{V}_H = \vec{V}_X + \vec{V}_Y$ e h is the ocean depth.

The magnetic field induced by the ocean \vec{b} can be classified, in a simplified way, into two components: toroidal and poloidal. The toroidal component is generated by electric currents, which close their circuits in planes such that these currents generate an induced magnetic field with a direction parallel to the surface of the ocean. This component can reach a magnitude of up to 100 nT, and it is confined between the surface of the ocean and the upper edge of the earth's crust. The poloidal component, in turn, is much weaker, with a magnitude between 1 and 10 nT. It arises through the electric currents that close their circuits in planes perpendicular to those related to the currents that give rise to the toroidal component of the induced magnetic field \vec{b} . However, this component extends from regions close to the ocean to satellite altitudes (TYLER et al. 2003, MANOJ et al. 2006, and the references within).

The toroidal and poloidal components are also affected by two types of geomagnetic fluctuations: periodic (lunar and solar variations) and transient disturbances (geomagnetic storms), as discussed by Longuet-Higgins et al. 1954. In geomagnetically quiet periods, induced magnetic fields are much more easily detected compared to disturbed periods (TYLER et al. 2003). In their work, Manoj et al. (2011) report that it was only possible to detect these induced magnetic fields because the analyzed event occurred on a geomagnetically quiet day. This fact imposes a challenge for methodologies that somehow assist in the geomagnetic detections.

4. DATA

A computational tool was developed to graphically analyze the local geomagnetic behavior, which possibly suffered variations caused by seismic and oceanic forcing. The algorithm was written in the MATLAB language with the input signals for the 5 most geomagnetically quiet days of February, the event day, and the sea-level data.

The data used in this work are magnetometer records of the H- and Z-component, provided by the LISN project (Low Latitude Ionospheric Sensor Network, <http://lisn.igp.gob.pe/>). Figure 4 shows the geographic distributions of the magnetic observatories and the tide gauge station, Callao La Punta (call). The star symbol denotes the epicenter of the Maule earthquake (2010).

The information about magnetic observatories is shown in Table 1. This table is composed of the name of the magnetic observatory, the IAGA code, Latitude, Longitude, and radial distance from the epicenter for each magnetic observatory. The sea level variation data were obtained from the Sea Level Station Monitoring Facility website available at <http://www.ioc-sealevelmonitoring.org/station.php>. The information about magnetic observatories is shown in Table 1. This table is composed of the name of the magnetic observatory, the IAGA code, Latitude, Longitude, and radial distance from the epicenter for each magnetic observatory. The sea level variation data were obtained from the Sea Level Station Monitoring Facility website available at <http://www.ioc-sealevelmonitoring.org/station.php>. The call station was selected because its location is close to the chosen magnetic observatories (see Figure 4), located at -12.07° in Latitude and -77.17° in Longitude, and 2681.35 km away from the epicenter. According to the US government institution National Tsunami Warning Center (NOAA/NWS), the tsunami wavefront arrived at Callao La Punta station at 10:34 UT on February 27, 2010.



Figure 4 - Geographic layout of the magnetic observatories (red circle symbol), the tide measurement station (green circle symbol), and the earthquake/tsunami epicenter (star symbol). Source: Modified from Google Maps (2020).

Table 1 - Magnetic observatories of the LISN project, their geographical coordinates, and their radial distances from the epicenter. Source: the authors.

Magnetic observatories of the LISN project			
Geomagnetic observatory, IAGA Code	Lat. (°)	Long. (°)	Epicentral Distance (km)
Ancon, ANC	-11,78	-77,15	2712,83
Huancayo, HUA	-12,05	-75,33	2658,96
Leticia, LET	-4,19	-69,94	3531,51

To determine the Sq curve, it was verified through the Kp index, available at <http://wdc.kugi.kyoto-u.ac.jp/kp/index.html>, the five geomagnetically quiet days of February, being them: 05, 09, 20, 21, and 28, the event day must be excluded. To remove the nocturnal variation average related to the ionosphere variability, the arithmetic mean was carried out between 23: 00-03: 00 (LT) for each day, and this mean was removed from the data. The average between the quiet days was also taken from the data, to obtain the characteristic Sq curve of February 2010.

Finally, the Sq curve was removed from the signal referring to the event day in order to remove the recurring daily magnetic field variations due to the Earth's rotation. These procedures were performed to emphasize the magnetic variations induced by ocean currents and by GWs/AGWs. With the filtered data in hand, we performed the analysis that will be presented and discussed in the next section.

5. RESULTS AND DISCUSSION

Figure 5 shows the geomagnetic disturbances resulting from GWs/AGWs and the oceanic electrical currents induced by the Maule tsunami (2010), as will be discussed later.

The results obtained here were done by filtering the data, referring to the magnetic component, baseline Sq, and sea level data. Specifically, as shown in Figure 5, the top panel has two curves, one representing the event (in blue), and another, the Sq baseline (in black), in addition to five thinner black curves representing the five most geomagnetically quiet days. One can note that the Sq baseline is subtracted from the magnetic data for the event day to emphasize the tsunamigenic magnetic variations.

In the bottom panel, the residual magnetic data (blue curve) is defined as the difference between the event data with the removal of the Sq baseline and its polynomial adjustment. In addition, the bottom panel contains sea level data (orange curve), allowing the arrival of the tsunami to be used as a reference for the analysis of the magnetic residual data. In the Callao La Punta region, tsunami waves arrived on the coast of Peru at 10:34 UT (four hours after the tsunami onset) with an amplitude of 0.69 m in height.

In the bottom panel of each figure, it is possible to notice that, before the arrival of the tsunami, the residual magnetic data showed smoothed variations (less than $|2|$ nT) and, after that, the magnetic variations appear amplified, with a similar signature pattern of the sea-level data related to the tsunami propagation. In the residual magnetic data, we look for wave packets in the form of inverted N-shaped during or after the tsunami arrival, since we would not expect magnetic variations of external origin, because this event occurred on a very geomagnetically quiet day. If these wave packs exist, we can determine that there is a possibility of tsunamigenic origin. It is possible to notice that these inverted N-shaped amplifications were identified in the geomagnetic data of all the observatories studied here, in both H- and Z-components. Also, similarities between the residual magnetic data and the sea-level data increase the possible association between them during the tsunami. These amplifications in the magnetic residuals appear from 6 to 100 minutes after the tsunami arrival in the magnetic observatories.

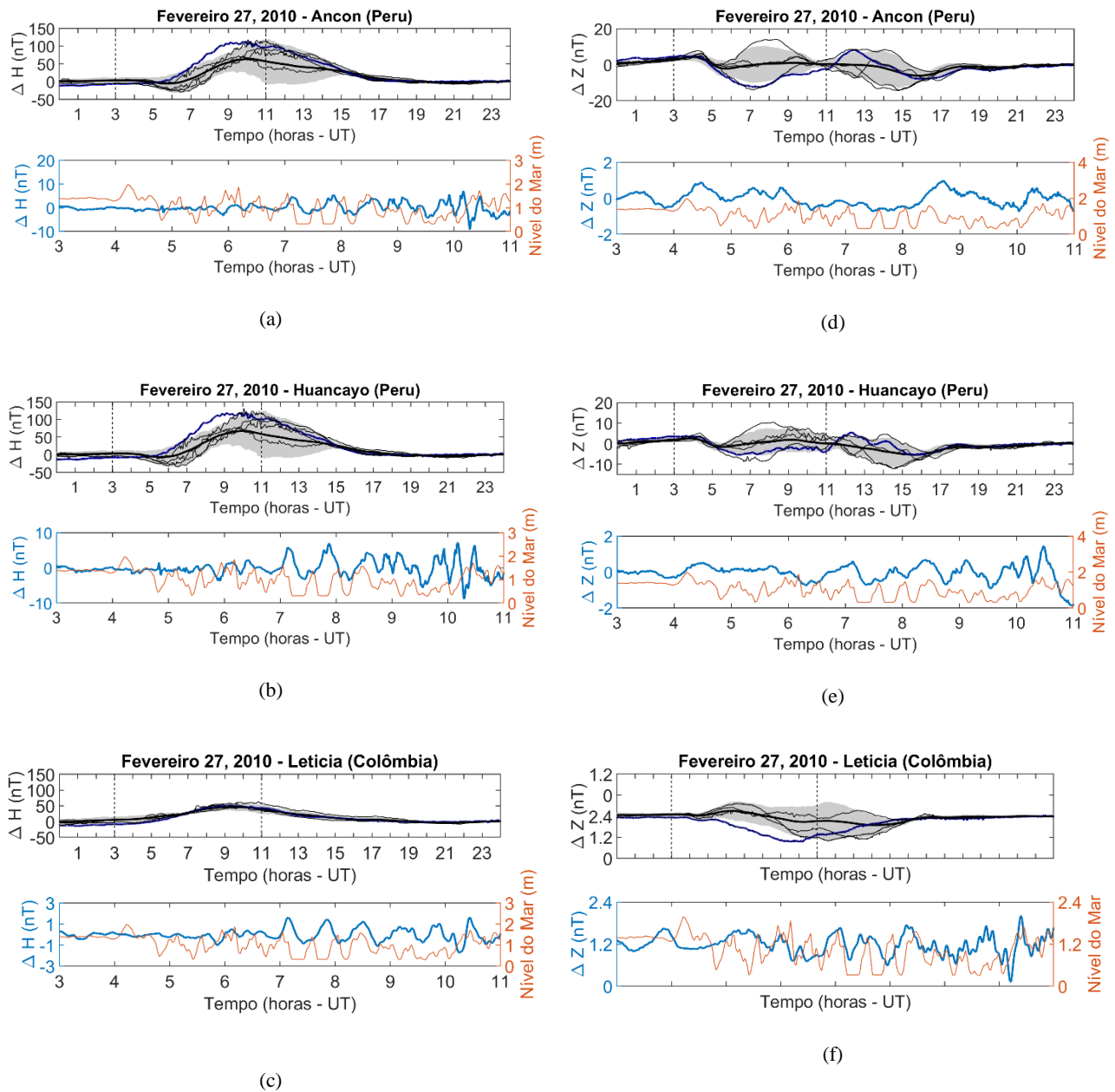


Figure 5 - The H-component (a, b, c) and Z-component (d, e, f) obtained at the magnetic observatory of Ancon, Huancayo, and Leticia, respectively, and their residual analyzes, with the use of filtering by removing the baseline S_q (top panel: black curve). The S_q baseline is calculated using the five most geomagnetically quiet days (top panel: curves with thinner thickness in black). The filtering process was applied to raw data zero centered (upper panel: blue curve). The bottom panel shows the residual magnetic data (blue curve) obtained by subtracting the S_q baseline from the magnetic component. The orange curve corresponds to the measurement of the sea level in call. In both panels, on the vertical axis, the geomagnetic variation in nT and/or variation in sea-level in meters are shown, and on the horizontal axis, the time in hours, where the "0" is considered to be the tsunami onset, corresponding to 06:34 UT. Source: the authors.

This delay time is consistent with the time that GWs/AGWs propagate in the neutral atmosphere until they reach higher altitudes, that is, ionospheric altitudes (KHERANI et al. 2012).

6. CONCLUSION

Studies related to seismic and/or tsunamigenic magnetic variations have shown great potential to collaborate with scientific applications useful for research in the area of Seismic Climate.

Our results were able to identify amplified waveforms in the inverted N-shaped in magnetic data with a signature pattern similar to sea level data related to the propagation of tsunami waves. These magnetic signatures appeared 6 to 100 minutes after the tsunami wave arrival. The presence of amplified magnetic disturbances in the H- and Z-components associated with the arrival of the tsunami waves was detected in each of the magnetic observatories studied here. However, no distinction can be made between seismic or oceanic mechanisms.

In addition to the scientific purpose of studying the Seismic Climate, the practical importance of predicting and characterizing such phenomena is the potential for forecast earthquakes and/or tsunamis and, early warning of these catastrophes, which could prevent the death of probable thousands of people, since these induced fields could be detected up to two hours in advance, as shown by Klausner et al. 2014. Moreover, the occurrence of earthquakes and/or tsunamis, such as the Maule tsunami (2010), can generate ionospheric irregularities that can propagate to Brazilian territory. Currently, there is also a dependency on general society to use satellite communication technologies, navigation and GPS positioning systems, space stations, complex electrical transmission systems, among other technological facilities that can be interrupted or impaired by ionospheric disturbances.

5. REFERENCES

- FARADAY, M. *Experimental researches in electricity*: Faraday, Michael, 1791-1867. London: Dent; New York: Dutton, 1922.
- IYEMORI, T.; NOSE, M.; HAN, D.; GAO, Y.; HASHIZUME, M.; CHOOSAKUL, N.; SHINAGAWA, H.; TANAKA, Y.; UTSUGI, M.; SAITO, A.; MCCREADIE, H.; ODAGI, Y.; YANG, F. *Geomagnetic pulsations caused by the Sumatra earthquake on December 26, 2004*. Geophysical Research Letters, v. 32, n. 20, L20807, 2005.
- KHERANI, E. A.; LOGNONNÉ, P.; HÉBERT, H.; ROLLAND, L.; ASTAFYEVA, E.; OCCHIPINTI, G.; COISSON, P.; WALWER, D.; DE PAULA, E. R. *Modelling of the total electronic content and magnetic field anomalies generated by the 2011 Tohoku-Oki tsunami and associated acoustic-gravity waves*. Geophysical Journal International, v. 191, n. 3, p. 1049-1066, 2012.
- KLAUSNER, V.; MENDES, O.; DOMINGUES, M. O.; PAPA, A. R. R.; TYLER, R. H.; FRICK, P.; KHERANI, E. A. *Advantage of wavelet technique to highlight the observed*

geomagnetic perturbations linked to the Chilean tsunami (2010). Journal of Geophysical Research: Space Physics, v. 119, n. 4, p. 3077-3093, 2014.

- LOGNONNÉ, P. L.; GARCIA, R.; CRESPON, F.; OCCHIPINTI, G.; KHERANI, E. A. *Seismic waves in the ionosphere*. Europhysics News, v. 37, n. 4, p. 11-14, 2006.
- LONGUET-HIGGINS, M. S.; STERN, M. E.; STOMMEL, H. M. *The electrical field induced by ocean currents and waves, with applications to the method of towed electrodes*. Massachusetts Institute of Technology and Woods Hole Oceanographic Institution, 1954. 1-37 p.
- MANOJ, C.; KUVSHINOV, A.; MAUS, S.; LUHR, H. *Ocean circulation generated magnetic signals*. Earth Planets and Space, v. 58, n. 4, p. 429-437, 2006.
- MANOJ, C.; MAUS, S.; CHULLIAT, A. *Observation of magnetic fields generated by tsunamis*. Eos, Transactions, American Geophysical Union, v. 92, n. 2, p. 13, 2011.
- MEDEIROS, ALEXANDRE. *Terremotos e Ondas Sísmicas Transversais, Longitudinais e Complexas*. Física e Astronomia Alexandre Medeiros, BLOG. Disponível em: <http://alexandremedeirosfisicaastronomia.blogspot.com/2011/11/terremotos-e-ondas-sismicas.html>. Acesso em: 03/10/2019.
- Teixeira, W.; Taioli, F.; Fairchild, T.; Toledo, C. *Decifrando a Terra*. São Paulo, Brasil: Companhia Editora Nacional, 2 ed. 2009.
- TSUGAWA, T., *Concentric Waves Appear at 300 km Altitude after the 2011 Tohoku Earthquake*. National Institute of Information and Communications Technology (NICT) News, Japan, v. 12, n. 411, 2011.
- TYLER, R. H.; MAUS, S.; LUHR, H. *Satellite observations of magnetic fields due to ocean tidal flow*. Science, v. 299, n. 5604, p. 239-241, 2003.
- TYLER, R. *A simple formula for estimating the magnetic fields generated by tsunami flow*. Geophysical Research Letters, v. 32, n. L09608, 2005.

6. ACKNOWLEDGEMENTS

The authors would like to thank CNPq for the productivity grant (305249/2018-5) and for scientific initiation fellows (800038/2014-2, 138978/2015-8, and 126499/2019-5).

Received in: 10/07/2020

Accepted for publication in: 09/12/2020